ISSN 0031-918X, Physics of Metals and Metallography, 2017, Vol. 118, No. 10, pp. 1022–1030. © Pleiades Publishing, Ltd., 2017.
Original Russian Text © Yu.I. Borisova, V.A. Dudko, V.N. Skorobogatykh, I.A. Shchenkova, R.O. Kaibyshev, 2017, published in Fizika Metallov i Metallovedenie, 2017, Vol. 118, No. 10, pp. 1072–1080.

STRENGTH AND PLASTICITY

Microstructural Changes in Cast Martensitic Steel after Creep at 620°C

Yu. I. Borisova[a], V. A. Dudko[a, *], V. N. Skorobogatykh[b], I. A. Shchenkova[b], and R. O. Kaibyshev[a]

[a] *Belgorod State University, ul. Pobedy 85, Belgorod, 308034 Russia*

[b] *Central Research Institute of Machine-Building Technology, ul. Sharikopodshipnikovskaya 4, Moscow, 115088 Russia*

**e-mail: dudko@bsu.edu.ru*

Received December 19, 2016; in final form, December 28, 2016

Abstract—Microstructural changes in the cast steel GX12CrMoWVNbN10-1-1 (Fe–0.11 C–0.31 Si–0.89 Mn–9.57 Cr–0.66 Ni–1.01 Mo–1.00 W–0.21 V–0.06 Nb–0.05 Cu–0.05 N in wt %) have been investigated after tests for long-term strength at a temperature of 620°C in the range of stresses of 120–160 MPa. Upon short-term creep (up to 5000 h), the tempered troostite structure and distribution of particles of proeutectoid constituents change insignificantly, except for the precipitation of particles of the Laves phase ~100 nm in size along boundaries of laths, blocks, packets, and initial austenite grains. Upon long-term creep (to 10000 h), the tempered troostite partially transforms into the subgrain structure, which is accompanied by a decrease in the dislocation density from 6.4×10^{14} to 3.1×10^{13} m^{-2} and connected with growth of sizes of $M_{23}C_6$ carbides of 105–150 nm and particles of the Laves phase to 380 nm, due to the dissolution of these particles located along path boundaries. Upon long-term creep, the average size of V(C,N) particles increases from 45 to 64 nm (while Nb(C,N) particles increase from 48 to 87 nm), and the Nb content in V-enriched carbonitrides and the V content in Nb-enriched *M*(C,N) particles substantially decrease. No formation of the *Z* phase has been revealed. The combination of *M*(C,N) nanoparticles with the presence of W in the solid solution has been found to be responsible for the enhanced high-temperature strength of the steel.

Keywords: creep, heat-resistant martensitic steels, carbides, orientation relationships

DOI: 10.1134/S0031918X1708004X

INTRODUCTION

Nowadays progress in development of coal-fired power-generating units is connected with elaboration of new martensitic steels containing 9–12 wt % Cr with enhanced creep resistance. Growth in the steam parameters from conventional (18 MPa, 530–540°C) to ultrasupercritical (30 MPa, 600°C) values became possible due to the development of new high-chromium steels with enhanced high-temperature strength and their use in the construction of boilers, main steam pipelines, and steam turbines [1–3]. This made it possible to increase the efficiency of power plants by 6–8% [4]. The growth of steam parameters to ultrasupercritical values results in requirement to strengthen not only steels employed in boilers and pipelines, but also cast steels used to fabricate castings of turbine casings, valves, inlet headers and pipes, and fittings. This led to the need to fabricate these parts of cast modifications of high-chromium steels, such as steel 12Kh10M1V1FBR, which is a Russian analog of the well-known cast steel GX12CrMoWVNbN10-1-1. As is known, the ability of steels with 9–12 wt % Cr to resist creep is determined by the ability of the tempered troostite structure to be retained under service conditions at elevated temperatures [4–8]. For this reason, the understanding of mechanisms of creep and degradation of the microstructure is of decisive importance in development and practical application of new martensitic steels as structural materials of thermal stations. Despite the wide use of high-chromium cast steels for production of equipment for power-generating units in Japan, European Union countries, the United States, and China, a limited number of works devoted to investigating microstructural changes upon long-term (time to failure ~10000 h and more) high-temperature creep are available [4, 8, 9]. It should be noted that cast modifications of steels with 9 wt % Cr contain an enhanced content of Ni that reduces the resistance of $M_{23}C_6$ carbides to coalescence upon creep, which unfavorably affects the long-term strength of these materials [5]. The purpose of this work is to analyze the effect of long-term creep with times to failure of up to 10000 h on the microstructure and phase composition of a cast steel GX12CrMoWVNbN10-1-1 at a temperature of 620°C.

EXPERIMENTAL

The material used for the investigation was cast steel GX12CrMoWVNbN10-1-1 (Fe–0.11 C–0.31 Si–

0.89 Mn–9.57 Cr–0.66 Ni–1.01 Mo–1.00 W–0.21 V–0.06 Nb–0.05 Cu–0.05 N in wt %), which was produced by the Voestalpine Giesserei Traisen Company (Austria). The steel was subjected to normalization from a temperature of 1100°C and tempering at a temperature of 730°C for 8 h with subsequent cooling in air. Tests for long-term strength of samples 10 mm in diameter with the working part 50 mm in length were conducted until failure at stresses of 120, 140, and 160 MPa at a temperature of 620°C. Structural studies were performed on samples after tempering and on longitudinal cross sections of the samples after creep using an Olympus GX71 optical microscope (Olympus LTD, Japan), a Quanta 600FEG scanning electron microscope (FEI, Hillsboro, Oregon) equipped with an analyzer of electron backscatter diffraction and a system of constructing misorientation maps (orientation-image microscopy), and a JEM-2100 transmission electron microscope (TEM) (JEOL Ltd., Tokyo, Japan) with an integrated and communications automatic attachment for energy dispersive analysis (Oxford Instruments, Oxfordshire, Great Britain). A polished section for optical microscopy was etched in a solution of 2% HNO_3 + 1% HF + 97% H_2O. TEM foils were prepared by the method of jet electrochemical polishing using a 10% solution of perchloric acid in acetic acid. The size of the grain/subgrain was determined by the intercept method from photographs obtained using TEM. The dislocation density was estimated by calculating individual dislocations in the body of the grain/subgrain using at least six randomly chosen photographs. Particles at carbon replicas were identified on the TEM using energy dispersive analysis.

RESULTS

Microstructure after Normalization and Tempering

Figures 1 and 2 display a characteristic microstructure of the steel GX12CrMoWVNbN10-1-1 after quenching and tempering. Quenching from a relatively high temperature that was 50 K higher than the heating temperature for quenching of steels of the P911/E911 type [12] gave rise to typical structure of packet martensite. Within the prior austenite grain (PAG), packets, blocks, and laths of martensite are observed [5–7] (Figs. 1, 2). The PAG size estimated with the help of optical microscopy was ~110 μm (Fig. 1), which nearly three to five times larger than in wrought high-chromium steels [6, 7]. Very large blocks in the form of long bands are observed. At the same time, the average distance between high-angle boundaries (HABs) calculated from misorientation maps was 4.2 μm (Fig. 2a), which is close to the analogous size for wrought high-chromium steels [6, 7]. The transverse size of laths was 332 nm (Fig. 2b), which is also typical for wrought steels containing 9 wt % Cr [6, 7]. Inside laths, the observed high dislocation density was 6.4×10^{14} m^{-2}. Heat treatment led to the precipitation

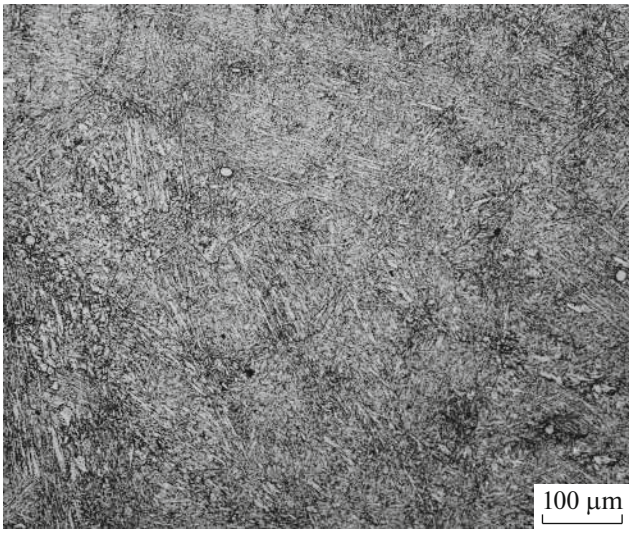

Fig. 1. Microstructure of steel GX12CrMoWVNbN10-1-1 after quenching at 1100°C and tempering at 730°C. Optical metallography.

of particles of proeutectoid constituents (Figs. 2b, 2c). *MX* (where *M* is vanadium and/or niobium and *X* is carbon and nitrogen) carbonitrides precipitated upon tempering are uniformly distributed in the ferrite matrix. The well-known [5–7, 10–14] two-phase separation of carbonitrides into V- and Nb-enriched particles takes place (Fig. 2d). The average sizes of V(C,N) and Nb(C,N) carbonitrides are 45 and 48 nm, respectively. It should be noted that the average chromium content in *M*(C,N) carbonitrides is 25 at % and this amount of Cr is limiting for this phase [15]. The growth of the Cr content above 25 at % results in the rearrangement of the lattice of *M*(C,N) carbonitrides into the lattice of the Z phase representing (VCr)N nitride [15]. It should be noted that the size of *M*(C,N) carbonitrides is nearly 60% larger than in steel P911/E911 [12].

Lath boundaries are decorated by $M_{23}C_6$ particles with an average size of 105 nm (Fig. 3). $M_{23}C_6$ (where *M* is chromium and iron) carbides have the shape slightly extended along the boundaries. The chemical composition of $M_{23}C_6$ carbides is identical to that in steels of the P911/E911 type [7, 12, 14, 16–18].

In Fig. 3, $M_{23}C_6$ carbides located at low-angle lath boundaries are shown in dark and bright fields. It follows from pointlike electron diffraction patterns that the crystallographic plane $(211)_\alpha$ of the matrix is parallel to the plane $(012)_{M_{23}C_6}$ of carbide. The direction of electron beam coincides with the axis $[12\bar{1}]_{M_{23}C_6}$ of the carbide zone and the $[351]_\alpha$ axis of the ferrite zone. Consequently, $M_{23}C_6$ carbides have the orientation relationship

$$(211)_\alpha \| (012)_{M_{23}C_6}, \quad [3\bar{5}1]_\alpha \| [12\bar{1}]_{M_{23}C_6}. \qquad (1)$$

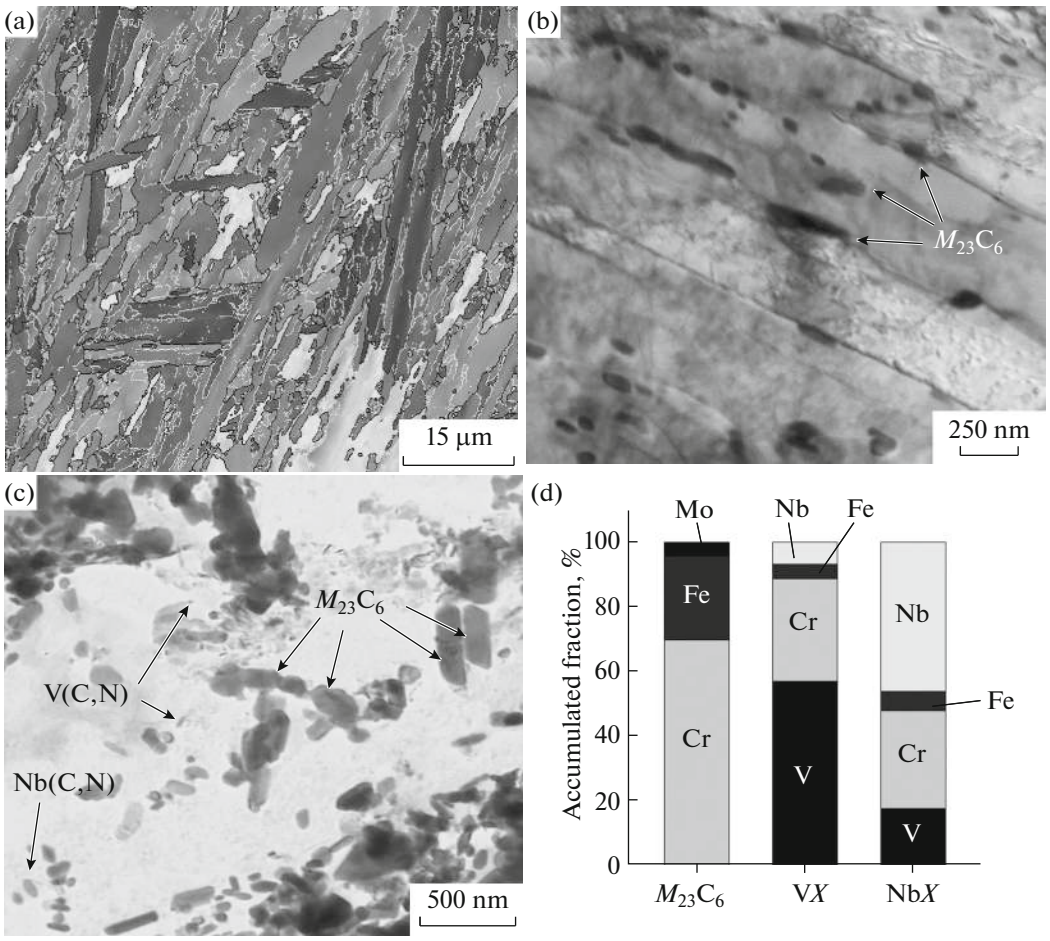

Fig. 2. Microstructure of steel GX12CrMoWVNbN10-1-1 after quenching at 1100°C and tempering at 730°C: (a) misorientation map (boundaries with misorientations of less and more than 15° are shown by white and black lines, respectively); (b) lath structure (TEM); (c) second-phase particles on carbon replica; and (d) average chemical composition (at %) of second-phase particles.

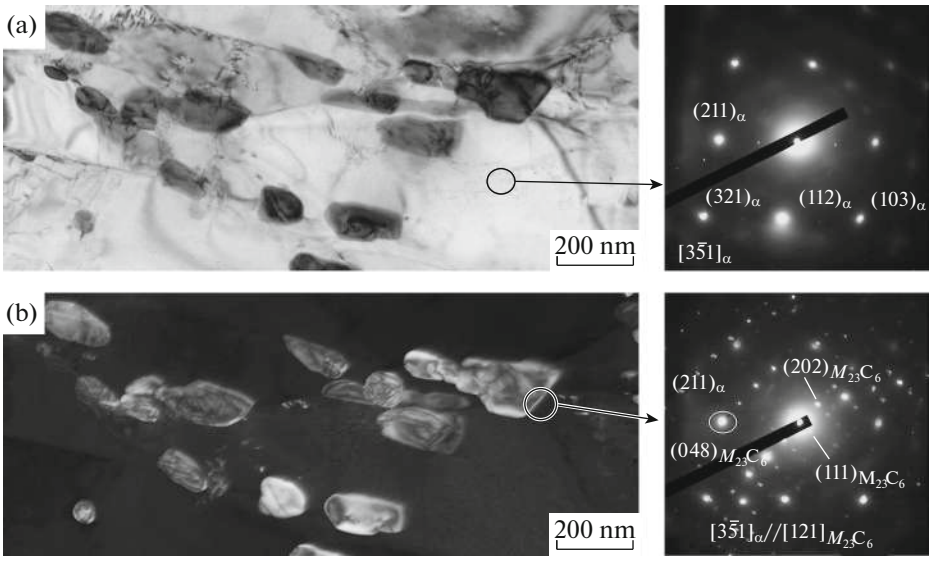

Fig. 3. Particles of $M_{23}C_6$ carbides along lath boundaries in steel GX12CrMoWVNbN10-1-1 after quenching at 1100°C and tempering at 730°C: (a) bright field and (b) dark field.

Table 1. Results of tests for creep of the steel GX12CrMoWVNbN10-1-1

Stress, MPa	Time to failure, h	Relative elongation, %	Relative reduction of area, %	Relative reduction of area at sites of cutting foils, %
120	10024	5.9	32.9	5.9
140	5373	9.6	38.8	13
160	1347	15.3	74.6	15.3

The orientation relationships between $M_{23}C_6$ carbides and the matrix in martensitic steels were analyzed in detail in [17, 18]. In [18], it was shown that, between $M_{23}C_6$ carbide particles and α-Fe particles, the Kurdjumov–Sachs (2) and Nishiyama–Wassermann (3) orientation relationships are satisfied as follows:

$$(011)_\alpha \| (111)_{M_{23}C_6}, \quad [\bar{1}1\bar{1}]_\alpha \| [01\bar{1}]_{M_{23}C_6} \qquad (2)$$

and

$$(011)_\alpha \| (111)_{M_{23}C_6}, \quad [100]_\alpha \| [01\bar{1}]_{M_{23}C_6}. \qquad (3)$$

Each of the orientation relationships with allowance for the symmetry of crystals can exhibit a certain number of equivalent variants. For cubic crystals, there are $24 \times 24 = 576$ methods of conjugating planes and the directions of two crystals by which the conditions of parallelism are satisfied. They form 24 different variants of misorientations, each of which can be described by 24 methods [19]. As a rule, the true solution is taken to be the one in which the angle of rotation is minimum (when the misorientation is described in the form of angle–rotation axis). It was shown [19] that, for the Kurdjumov–Sachs and Nishiyama–Wassermann orientation relationships, the misorientations are equal to 42.85° ⟨0.968 0.178 0.178⟩ and 45.98° ⟨0.976 0.083 0.201⟩, respectively. The orientation relationship (1) yields the misorientation 42.09° ⟨0.976–0.132–0.174⟩, which corresponds to the Kurdjumov–Sachs orientation relationship. No particles of the Laves phase were detected after tempering because the tempering temperature is higher than the solvus temperature of the Laves phase [5, 12, 20, 21].

Tests for Creep

Stresses at tests for creep were chosen so as to reach a time to failure of 1000, 5000, and 10000 h. The time to failure, elongation after failure, relative reduction of area, and estimate of relative reduction of area at the site of cutting foils for electron microscopy are listed in Table 1. A tenfold increase in the time to failure with a decrease in the applied stresses from 160 to 120 MPa leads to nearly a twofold decrease in the plasticity and a relative reduction in the area.

In the literature, a limited body of data on the long-term strength at 620°C of high-chromium steels close in chemical composition are available [22]. However, the obtained data unambiguously indicate that the given steel exhibits a higher creep resistance than the previous generation of steel GX12CrMoVNbN9-1, which represents a cast version of steel P91. The time to failure of samples of steel GX12CrMoVNbN9-1 at 600°C [22] and steel GX12CrMoWVNbN10-1-1 at 620°C is almost the same at all three values of stresses. Moreover, at 620°C, steel GX12CrMoWVNbN10-1-1 exhibits a time to failure that is approximately 50% higher than in the wrought steel P911/E911 [22] based on which it was created.

Microstructure after Tests for Creep

The results of a quantitative analysis of the microstructure are listed in Table 2. The microstructure of steel GX12CrMoWVNbN10-1-1 after creep at 620°C is shown in Fig. 4.

Creep exerts no influence on the distance between HABs that remains to be 4.2 μm after all testing regimes (Figs. 4a, 4c), which correlates with data on

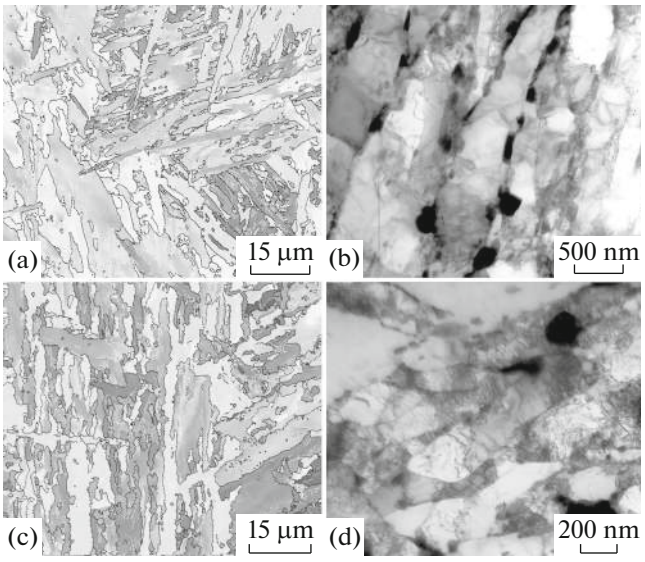

Fig. 4. Characteristic microstructure in the working part of samples of steel GX12CrMoWVNbN10-1-1 after creep at 620°C: (a) and (b) misorientation map and lath structure (TEM) after tests at 160 MPa for 1347 h; (c) and (d) misorientation map and lath structure (TEM) after tests at 120 MPa for 10024 h.

Table 2. Parameters of microstructure of the steel GX12CrMoWVNbN10-1-1 after heat treatment and creep at 620°C in different regimes

Parameters	Tempering	Applied stresses, MPa/Time to failure, h		
		160/1347	140/5373	120/10024
Transverse size of laths/subgrains, nm	332 ± 46	500 ± 70	630 ± 88	550 ± 77
Distance between HABs, μm	4.2 ± 0.8	4.0 ± 0.8	4.2 ± 0.8	3.9 ± 0.7
Fraction of special boundaries, %	18	13.8	11.3	16.8
Dislocation density, m^{-2}	6.4×10^{14}	4.2×10^{14}	1.2×10^{14}	3.1×10^{13}
Average size of $M_{23}C_6$, nm	105 ± 24	98 ± 22	110 ± 24	150 ± 33
Average size of V(C,N), nm	45 ± 23	45 ± 23	45 ± 23	64 ± 33
Average size of Nb(C,N), nm	48 ± 25	48 ± 25	51 ± 27	87 ± 45
Average size of Fe_2(W,Mo), nm	–	94 ± 15	231 ± 37	386 ± 62

the structural changes in the process of creep in other steels [12, 13]. It was also established that creep does not lead to a change in the fraction of special boundaries (Table 2). Based on the behavior of structural changes, one can clearly distinguish the region of short-term creep at stresses of 140 MPa and higher, and the region of long-term creep at stresses 120 MPa and below [23–25].

Upon short-term creep, the lath structure is retained up to failure, although the transverse size of laths increases by approximately twofold. The dislocation density decreases by factors of 1.5 and 4 at 160 and 140 MPa, respectively. The stability of the tempered troostite structure upon creep is caused by the fact that the size of M(C,N) carbonitrides remains almost unaltered upon creep and $M_{23}C_6$ carbides located at lath boundaries coalesce and do not dissolve. In addition, rounded particles of the Laves phase precipitate at lath boundaries, which likewise contributes to the Zener drag force of migration of low-angle boundaries [6, 23, 26]. It should be noted that, at 160 MPa, fine Fe_2W particles of the Laves phase precipitate along lath boundaries, which additionally stabilizes the lath structure due to an enhancement in the Zener drag force [6, 23]. At 140 MPa, particles of the Laves phase located along HABs of packets and PAGs has time to coalesce at the expense of the dissolution of particles of this phase located along the lath boundaries, which depreciate the contribution of the Laves phase to the total Zener drag force [6, 23]. The lath structure is retained after creep $>5 \times 10^3$ h due to the high Zener drag force of $M_{23}C_6$ carbides located along lath boundaries [6, 23]. The structure after long-term creep differs significantly from that after short-term creep. At 120 MPa, the tempered troostite structure partially transforms into the subgrain structure, which is accompanied by a 20-fold decrease in the density of lattice dislocations. However, the lath structure is largely retained, and the formation of round subgrains is only observed in some places. As distinct from short-term creep, the number of $M_{23}C_6$ particles located along lath boundaries decreases and makes the main contribution to the Zener drag force [6, 23].

The dissolution of these carbides occurs in the process of the coalescence of large $M_{23}C_6$ carbides located along HABs of blocks and PAGs. However, this does not result in the intense migration of low-angle boundaries, despite the growth in the average size of $M_{23}C_6$ carbides by a factor of 1.5. At the same time, particles of the Laves phase located along HABs of blocks and PAGs coalesce intensely. The sizes of the majority of particles of this phase become greater than 1 μm. It is known [23, 27] that the large particle size assists in the formation of cracks upon creep due to their nucleation at HABs, which leads to a reduction in the relative elongation by a factor of three or more. The chemical composition of particles of the Laves phase is characterized by a large Mo/W ratio that is substantially higher than in P911 (~1.8) steel [12]. As the time to failure increases and the intense coalescence of particles of the Laves phase develops, this ratio decreases and remains higher than ~3. This means that a larger part of W remains in the solid solution, since this element does not precipitate in the composition of $M_{23}C_6$ carbides and only one third of W goes to form the Laves phase. This behavior is unusual for steels with 9 wt % Cr [28]. Consequently, the presence of Ni in the ferrite affects the ratio of Mo/W by increasing it, which is opposite to the influence of Co [12]. The retention of more than two-thirds of W in the ferrite is most likely responsible for the higher long-term strength (at 620°C) of steel GX12CrMoWVNbN10-1-1, compared to steel P911/E911, since in [22, 23], it was shown that the processes of the transformation of the tempered troostite structure into the subgrain structure develop after W leaves the ferrite with the precipitation of the Laves phase and additional $M_{23}C_6$ carbides in the composition.

The size of M(C,N) carbonitrides increases by 40% after long-term creep for 10 024 h, which facilitates the dislocation climb and, hence, a reaction between lattice dislocations and dislocations that make up the lath

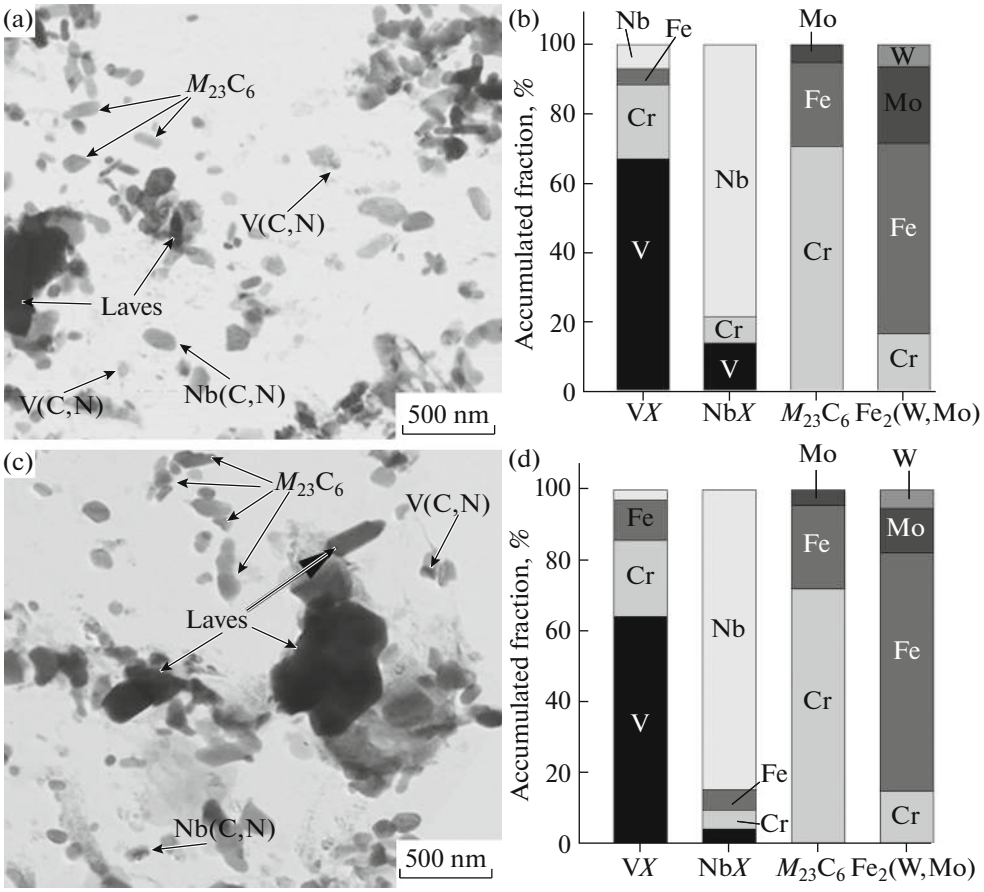

Fig. 5. Particles of proeutectoid constituents on carbon replicas and their average chemical composition in the steel GX12CrMoWVNbN10-1-1 after creep at 620°C: (a, b) at 160 MPa for 1347 h and (c, d) at 120 MPa for 10024 h (TEM).

boundaries. This reaction leads to a catastrophic decrease in the density of lattice dislocations and the transformation of lath boundaries (these are sources of high elastic stress fields) into subgrain boundaries. The latter either do not generate long-range stress fields at all or the magnitude of elastic stresses from them is four to six times smaller than from lath boundaries [23, 29, 30]. Upon creep, a considerable change in the chemical composition of M(C,N) carbonitrides occurs, which consists of a decrease in the Nb content in V-enriched carbonitrides and a decrease in the V content in Nb-enriched particles. At the same time, no formation of the Z phase was revealed. It should be noted that, in the opinion of some authors, the process of substituting nanoparticles of M(C,N) carbonitrides for particles of the Z phase about 1 μm in size in the process of creep, which is responsible for the loss of the ability of high-chromium steels to resist creep upon long-term service [15, 31]. The decrease in creep resistance of the steel GX12CrMoWVNbN10-1-1 is mainly caused by the dissolution of $M_{23}C_6$ carbides along lath boundaries.

These carbides play a significant role in preventing the reaction between lattice dislocations and dislocations that constitute lath boundaries [32] and a decisive role in retarding the migration of low-angle boundaries [6, 23, 26].

DISCUSSION OF RESULTS

Thus, at 620°C, steel GX12CrMoWVNbN10-1-1 demonstrated long-term strength, which is ~20% higher than in P911/E911 (wrought analog of this steel when the creep time is 10^4 h) [12, 22]. This is connected with features of the martensite structure (arising upon quenching) in steel with very coarse PAGs. As was shown previously [6, 7, 23, 26], the precipitation of $M_{23}C_6$ carbides and the Laves phase along HABs of the tempered troostite suppresses their migration. In this case, the Zener force retarding migration is three to five times greater than the sum of driving forces. The loss of creep resistance is connected with the development of dynamic recovery at the steady state and accelerated stages of creep, which results in the transition from short- to long-term creep [6, 23–25, 33]. Quenching creates a very favorable distribution of $M_{23}C_6$ carbides from the viewpoint of stability of the tempered troostite structure against trans-

Table 3. Calculated sizes of laths in the steel GX12CrMoWVNbN10-1-1 after creep at 620°C

Initial stress, MPa/ Time to failure, h	D, nm	D_{ss}, nm
120/10024	500	1017
140/5373	570	816
160/1347	550	697

formation into the subgrain structure. Furthermore, an additional precipitation of particles of the Laves phase along lath boundaries is observed, and a larger part of W remains in the solid solution. This appreciably slows down the rate of diffusion and, hence, dislocation climbs [5, 23] with the result that changes in the tempered troostite structure in the process of short-term creep are insignificant.

It was shown in [18] that the misfit parameter of lattices of $M_{23}C_6$ carbide and α-Fe matrix is 1.1% upon the fulfillment of the Kurdjumov–Sachs orientation relationship. Consequently, the carbide–matrix boundary in steel GX12CrMoWVNbN10-1-1 can be coherent. Calculations in [18] showed that the rate of growth in $M_{23}C_6$ carbides with coherent boundary is approximately twofold smaller than with incoherent boundary. This is probably due to the coherence of boundaries between $M_{23}C_6$ carbides and ferrite matrix that the size of carbide particles remains almost unaltered upon creep to ~5000 h. However, it seems likely that upon long-term creep, the coherence of carbide particles terminates abruptly and the coalescence rate increases sharply. The loss of the coherence upon creep can take place because of the incompatibility of the deformation at the particle/matrix boundary and the accumulation therein of geometrically necessary dislocations. The decrease in the number of particles of $M_{23}C_6$ carbides and the Laves phase at lath boundaries is mainly responsible for the development of the reaction between lattice dislocations and the dislocations that constitute lath boundaries, which results in the transformation of lath boundaries into subgrain boundaries. Coalescence of M(C,N) carbonitrides is likely to play an auxiliary role in acceleration of this process. This counts in favor of the above assumption that the density of lattice dislocations at 140 MPa decreases threefold for ~5000 h of creep and growth of the creep time by ~5000 h at 120 MPa additionally reduces the dislocation density by a factor of five. However, even in this case, the lath structure is partially retained, which can only be connected with the retardation of the migration of subgrain boundaries at the expense of nanoparticles of M(C,N) carbonitrides and the presence of W in the ferrite.

To test this assumption, let us estimate the thickness of laths, which is equilibrium for given conditions of creep and compare it with the experimentally observed thickness. It was established in [8] that the average size of laths/subgrains D becomes larger with an increase in the degree of deformation ε in terms of the empirical expression

$$\log D = \log D_{ss} + \log(D_0/D_{ss})\exp(-\varepsilon/0.12), \qquad (4)$$

where $D_{ss} = 10bG/(\sigma_0(1+\varepsilon))$ is the equilibrium size of subgrains at the steady-state creep stage; $\varepsilon = \Psi/(1-\Psi)$, where Ψ is the relative reduction of area measured at the site of cutting foils; D_0 is the transverse size of laths after tempering; b is the Burgers vector; σ_0 is the initial stress; and G is the shear modulus equal to 52 GPa at 620°C. The subgrain sizes D calculated according to expression (4) and equilibrium subgrain sizes D_{ss} after different creep regimes are listed in Table 3. The experimental transverse sizes of laths (Table 2) are in good correlation with the calculated data for D (Table 3). However, the equilibrium subgrain size D_{ss} is nearly 1.5–2 times larger than that measured after creep. Consequently, the equilibrium subgrain structure has no time to arise in steel GX12CrMoWVNbN10-1-1, even at creep for 10024 h. This is responsible for high creep resistance of the steel under study.

CONCLUSIONS

(1) Quenching from a temperature of 1100°C and subsequent tempering at 730°C led to the formation of coarse PAGs ~110 μm in size and martensite blocks in the shape of bands. The average distance between HABs was 4.2 μm, the lath size was 332 nm, and the dislocation density was $\rho = 6.4 \times 10^{14}$ m^{-2}. In the ferrite matrix, Nb(C,N) and V(C,N) carbonitrides with average sizes of 48 and 45 nm, respectively, are arranged; $M_{23}C_6$ carbides with average size 105 nm are located along boundaries of laths, PAGs, blocks, and packets.

(2) At short-term creep (to 5000 h), the troostite structure is retained without considerable changes up to failure, whereas upon long-term creep (10 000 h) its partial transformation into the subgrain structure occurs with a 20-fold decrease in the density of lattice dislocations.

(3) Upon tempering, $M_{23}C_6$ carbides precipitate with respect to the matrix according to the Kurdjumov–Sachs orientation relationship. At short-term creep, no significant coalescence of these carbides takes place, whereas upon long-term creep, their average size grows to 150 nm. The precipitation of particles of the Laves phase along boundaries of all types is observed after short-term creep and, after long-term creep, intense coalescence gives rise to individual coarse particles along HABs. A feature of the steel is the low content of W in particles of the Laves phase and its lack in $M_{23}C_6$ carbides.

(4) Short-term creep does not affect the size of M(C,N) carbonitrides, whereas long-term creep increases the size of Nb(C,N) and V(C,N) carbonitrides by 40%. No formation of the Z phase was revealed. Creep intensifies the two-phase separation of M(C,N) carbonitrides into V- and Nb-enriched carbonitrides, and Cr escapes Nb(C,N) particles.

ACKNOWLEDGMENTS

This work was supported by the Russian Scientific Foundation, agreement on grant no. 14-29-00173. The authors thank the Collective-Use Center "Diagnostics of Structure and Properties of Nanomaterials" of Belgorod State National Research University, which kindly supplied us with equipment for structural studies.

REFERENCES

1. R. Viswanathan and W. Bakker, "Materials for ultrasupercritical coal power plants—Boiler materials: Part 1," J. Mater. Eng. Perfor. **10**, 81–95 (2001).
2. R. Hanus, "Advanced 9–12% Cr Cast Steel Grades, Research–Foundry Process Development–Quality–Experience," *Proc. 4th Int. Conf. "Advances in Materials Technology for Fossil Power Plants"",* Hilton Head Island, South Carolina. 2004, pp. 638–651.
3. G. Golanski, "Influence of heat treatment on microstructure and properties of GX12CrMoVNbN9-1 cast steel," Arch. Found. Eng. **10**, 89–94 (2010).
4. S. C. Bose, K. Singh, A. K. Ray, and R. N. Ghosh, "Effect of thermal ageing on mechanical properties and microstructures of a standard GX12CrMoVWNbN 10-1-1 grade of cast steel for turbine casing," Mater. Sci. Eng., A **476**, 257–266 (2008).
5. F. Abe, T. U. Kern, and R. Viswanathan, *Creep Resistant Steels* (Woodhead Publishing in Materials, 2008).
6. V. A. Dudko, A. Belyakov, D. Molodov, and R. O. Kaibyshev, "Microstructure evolution and pinning of boundaries by precipitates in a 9% Cr heat resistant steel during creep," Metal. Mater. Trans. A **44**, 162–172 (2013).
7. A. E. Fedoseeva, V. A. Dudko, R. O. Kaibyshev, P. A. Kozlov, V. N. Skorobogatykh, and I. A. Shchenkova, "Microstructural changes in steel 10KhV9MFBR during creep for 40000 hours at 600°C," Phys. Met. Metallogr. **116**, 1047–1056 (2015).
8. Y. Qin, G. Götz, and W. Blum, "Subgrain structure during annealing and creep of the cast martensitic Cr steel G-X12CrMoWVNbN 10-1-1," Mater. Sci. Eng., A **341**, 211–215 (2003).
9. G. Götz, Y. Qin, and W. Blum, "Investigation of precipitation in cast martensitic annealed steel GX12CrMoVWNbN 10-1-1 by semiautomatic EDX-analysis in the scanning transmission electron microscope," *Proc 3rd Int. Conf. "Advances in Materials Technology for Fossil Power Plants,"* Univ. of Wales Swansea. 2001, pp. 155–163.
10. I. I. Gorbachev, V. V. Popov, and A. Y. Pasynkov, "Thermodynamic calculations of carbonitride formation in low-alloy low-carbon steels containing V, Nb, and Ti," Phys. Met. Metallogr. **115**, 69–76 (2014).
11. I. I. Gorbachev, V. V. Popov, and A. Y. Pasynkov, "Simulation of precipitate ensemble evolution in steels with V and Nb," Phys. Met. Metallogr. **116**, 356–366 (2015).
12. A. Kipelova, M. Odnobokova, A. Belyakov, and R. O. Kaibyshev, "Effect of Co on creep behavior of a P911 steel," Metall. Mater. Trans. A **44**, 577–583 (2012).
13. V. A. Dudko, A. E. Fedoseeva, A. N. Belyakov, and R. O. Kaibyshev, "Influence of the carbon content on the phase composition and mechanical properties of P92-type steel," Phys. Met. Metallogr. **116**, 1165–1174 (2015).
14. A. F. Fedoseeva, N. Dudova, U. Glatzel, and R. O. Kaibyshev, "Effect of W on tempering behavior of a 3% Co modified P92 steel," J. Mater. Sci. **51**, 9424–9439 (2016).
15. L. Cipolla, H. K. Danielsen, D. Venditti, P. E. di Nunzio, J. Hald, and M. A. J.Somers, "Conversion of MX nitrides to Z-phase in a martensitic 12% Cr steel," Acta Mater. **58**, 669–679 (2010).
16. M. I. Isik, A. Kostka, V. A. Yadley, K. G. Pradeep, M. J. Duarte, P. P. Choi, D. Raabe, and G. Eggeler, "The nucleation of Mo-rich Laves phase particles adjacent to $M_{23}C_6$ micrograin boundary carbides in 12% Cr tempered martensite ferritic steels," Acta Mater. **90**, 94–104 (2015).
17. K. H. Kuo and C. L. Jia, "Crystallography of $M_{23}C_6$ and M_6C precipitate in a low-alloy steel," Acta Metall. **33**, 991–996 (1985).
18. A. Y. Kipelova, A. N. Belyakov, and R. O. Kaibyshev, "The crystallography of $M_{23}C_6$ carbides in a martensitic 9% Cr steel after tempering, aging and creep," Philos. Mag. **93**, 2259–2268 (2013).
19. Y. He, S. Godet, and K. Jonas, "Observations of the Gibeon meteorite and the inverse Greninger–Troiano orientation relationship," J. App. Crystallogr. **39**, 72–81 (2006).
20. A. Y. Kipelova, A. N. Belyakov, R. O. Kaibyshev, V. N. Skorobogatykh, and I. A. Shchenkova, "Tempering-induced structural changes in steel 10Kh9K3V1M1FBR and their effect on the mechanical properties," Metal Sci. Heat Treat. No. **3**, 100-110 (2010).
21. V. A. Dudko, A. N. Belyakov, and R. O. Kaibyshev, "Effect of tempering on mechanical properties and microstructure of a 9% Cr heat resistant steel," Mater. Sci. Forum **706–709**, 841–846 (2012).
22. D. G. Robertson and S. R. Holdsworth, European Creep Collaborative Committee (ECCC), Data Sheet, Working Group 9–12%Cr steels, Cast Steel P91, Steel **E911**. 2006. pp.51–54.
23. A. F. Fedoseeva, N. Dudova, and R. O. Kaibyshev, "Creep strength breakdown and microstructure evolution in a 3% Co modified P92 steel," Mater. Sci. Eng., A **654**, 1–12 (2016).

24. H. Ghassemi-Armaki, R. P. Chen, K. Maruyama, and M. Igarashi, "Contribution of recovery mechanisms of microstructure during long-term creep of Gr.91 steels," J. Nucl. Mater. **433**, 23–29 (2013).
25. F. Abe, "Creep behavior, deformation mechanisms and creep life of modified 9 Cr–1 Mo steel," Metall. Mater. Trans. A **46**, 5610–5625 (2015).
26. A. Y. Kipelova, R. O. Kaibyshev, A. N. Belyakov, and D. Molodov, "Microstructure evolution in a 3% Co modified P911 heat resistant steel under tempering and creep condition," Mater. Sci. Eng., A **528**, 1280–1286 (2011).
27. W. Zhong, W. Wang, X. Yang, W. Li, W. Yan, W. Sha, W. Wang, Y. Shan, and K. Yang, "Relationship between Laves phase and the impact brittleness of P92 steel reevaluated," Mater. Sci. Eng., A **639**, 252–258 (2015).
28. A. Y. Kipelova, A. N. Belyakov, and R. O. Kaibyshev, "Laves phase evolution in a modified P911 heat resistant steel during creep at 923 K," Mater. Sci. Eng., A **532**, 71–77 (2012).
29. V. A. Dudko, A. N. Belyakov, and R. O. Kaibyshev, "Sources of high creep resistance of modern high-chromium martensitic steels," Dokl. Phys. Chem. **464**, 191–193 (2015).
30. R. Mishnev, N. Dudova, and R. O. Kaibyshev, "Low cycle fatigue behavior of a 10Cr–2W–Mo–3Co–NbV steel," Int. J. Fatigue **83**, 344–355 (2016).
31. R. O. Kaibyshev, V. N. Skorobogatykh, and I. A. Shchenkova, "Formation of the *Z*-phase and prospects of martensitic steels with 11% Cr for operation above 590°C," Metal Sci. Heat Treat. **52**, 90–99 (2010).
32. M. Mitsuhara, Sh. Yamasaki, M. Miake, H. Nakashima, M. Nishida, J. Kusumoto, and A. Kanaya, "Creep strengthening by lath boundaries in 9Cr ferritic heat resistant steel," Philos. Mag. Lett. **96**, 76–83 (2016).
33. N. Dudova, A. Plotnikova, D. Molodov, A. N. Belyakov, and R. O. Kaibyshev, "Structural changes of tempered martensitic 9% Cr–2% W–3% Co steel during creep at 650°C," Mater. Sci. Eng., A **534**, 632–639 (2012).
34. J. Hald and L. Korcakova, "Precipitate stability in creep resistant ferritic steels—Experimental investigations and modeling," ISIJ Int. **43**, 420–427 (2003).

Translated by I. Krasnov